

Effects of Casimir force on pull-in instability in micromembranes

R. C. BATRA¹, M. PORFIRI² and D. SPINELLO¹

¹ *Department of Engineering Science & Mechanics, Virginia Polytechnic Institute & State University - Blacksburg VA 24061, USA*

² *Department of Mechanical, Aerospace & Manufacturing Engineering, Polytechnic University - Brooklyn NY 11201, USA*

received 5 September 2006; accepted in final form 21 November 2006

published online 19 January 2007

PACS 03.65.Sq – Semiclassical theories and applications

PACS 07.10.Cm – Micromechanical devices and systems

PACS 85.85.+j – Micro- and nano-electromechanical systems (MEMS/NEMS) and devices

Abstract – We analyze pull-in instability of electrostatically actuated microelectromechanical systems, and study changes in pull-in parameters due to the Casimir effect. When the size of the device is reduced, the magnitude of the Casimir force is comparable with that of the Coulomb force and it significantly alters pull-in parameters. We model the deformable conductor as an elastic membrane and consider different geometries. Beyond a certain critical size the pull-in instability occurs with zero applied voltage, and the device may collapse during the fabrication process.

Copyright © EPLA, 2007

Introduction. – Electrostatically actuated microelectromechanical systems (MEMS) are becoming increasingly useful in many applications such as switches, micro-mirrors and micro-resonators, see, *e.g.*, [1–3]. At the microscopic scale the electrostatic actuation may dominate over other kinds of actuation. Most of the electrostatically actuated systems [4] are comprised of a conductive deformable plate suspended over a rigid ground plate. An applied electric voltage between the two conductors results in the deflection of the elastic plate, and a consequent change in the system capacitance. The applied electrostatic voltage has an upper limit beyond which the two plates snap together and the device collapses. This phenomenon is called pull-in instability and the corresponding voltage the pull-in voltage; it was simultaneously observed experimentally by Taylor [5] and Nathanson *et al.* [6].

With the decrease in device dimensions from the micro to the nanoscale additional forces on nanoelectromechanical systems (NEMS), such as the Casimir force [7,8], should be considered. The Casimir force represents the attraction of two uncharged material bodies due to modification of the zero-point energy associated with the electromagnetic modes in the space between them. The existence of the Casimir force poses a severe constraint on the miniaturization of electrostatically actuated devices. At the nanoscale, the Casimir force may overcome elastic restoring actions in the device and lead to the plates' sticking

during the fabrication process. An important feature of the Casimir effect is that even though its nature is quantistic, it predicts a force between macroscopic bodies.

van der Waals forces are related to electrostatic interaction among dipoles at the atomic scale [9]. Whereas the Casimir force between semi-infinite parallel plates depends only on the geometry, van der Waals forces depend on material properties of the media. The Casimir force is effective at longer distance than van der Waals forces [9]. van der Waals forces are accounted for in NEMS where interactions occur at the atomic scale, as for example in carbon nanotubes [10]. van der Waals forces are not considered in the work presented below.

Here, we analyze the effect of the Casimir and the Coulomb forces on the pull-in parameters of NEMS for a large variety of common two-dimensional (2-D) geometries. We show that beyond a critical size, the pull-in instability occurs at zero voltage. This means that the system collapses during the manufacturing process. We also analyze symmetry-breaking in annular membranes due to the combined effects of the Coulomb and the Casimir forces. Different investigators have studied sticking in MEMS, but they did not consider the combined effect of the Casimir and the Coulomb forces. In [11,12] a rectangular membrane using the 1-D distributed model and considering nonlinear stretching effects has been studied, while in [13] a lumped one degree-of-freedom (d.o.f.) model has been used to analyze the stiction phenomenon

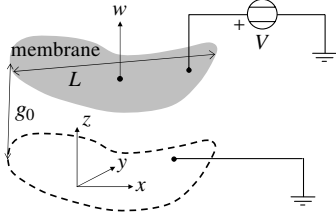


Fig. 1: Sketch of the electrostatically actuated device.

between two conductors made of different materials. In [14] the effect of Casimir force on pull-in parameters of NEM switches has been studied through a reduced one d.o.f. model.

In this work effects of surface roughness and surface curvature [12,15], temperature and finite conductivity [16] on the Casimir force are not considered. However, we note that for two metallic surfaces separated by $0.6\ \mu\text{m}$ – $6\ \mu\text{m}$, finite conductivity and surface roughness corrections can be as high as 20% and 20%–30% of the net Casimir force at the nearest points [17] respectively.

Formulation of the boundary-value problem. – Referring to the geometry depicted in fig. 1, we assume that the deformable electrode in the undeformed configuration is a plate-like body, and that the initial gap g_0 between the two conductors and the thickness h of the deformable plate are much smaller than its characteristic length L , with $h/L < 1/400$. Accordingly [4], we assume that the rigidity due to in-plane stretching dominates over the bending stiffness in carrying the external load. Under these assumptions, we model the deformable plate as a linear elastic membrane.

From an electrical point of view, the system behaves as a variable gap capacitor. The magnitude f_e of the electrostatic force acting on the deformable electrode along its normal is given by [4] $f_e = -\epsilon_0 \|\nabla\psi\|^2/2$, where ϵ_0 is the vacuum dielectric constant, ψ the electrostatic potential, ∇ the gradient operator, and $\|\cdot\|$ the Euclidean norm. The electrostatic potential satisfies the Laplace equation in the region $\Omega \times (0, g)$ with boundary conditions $\psi|_{z=0} = 0$, $\psi|_{z=g} = V$, where Ω is the 2-D region occupied by the membrane, $g = g_0 + w$ is the gap between the two conductors, w the displacement field, g_0 the initial gap, and V the applied voltage (see fig. 1). By nondimensionalizing the in-plane Cartesian coordinates x, y with respect to L , the vertical coordinate z and the displacement field w with respect to the initial gap g_0 , and the potential field with respect to V the Laplace equation for the electrostatic potential becomes

$$\delta^2 \left(\frac{\partial^2 \hat{\psi}}{\partial \hat{x}^2} + \frac{\partial^2 \hat{\psi}}{\partial \hat{y}^2} \right) + \frac{\partial^2 \hat{\psi}}{\partial \hat{z}^2} = 0. \quad (1)$$

Here, the aspect ratio of the device $\delta = g_0/L$ has been introduced, and nondimensional quantities have been denoted with a superimposed hat. We assume that $\delta \ll 1$,

and neglect the term multiplying δ^2 . Then, the solution of the electrostatic problem is $\psi(x, y, z) = Vz/(g_0 + w(x, y))$. The electrostatic force acting on the deformable electrode is given by

$$f_e = -\frac{\epsilon_0 V^2}{2g_0^2 (1 + \hat{w})^2} \left(1 + \delta^2 \left(\left(\frac{\partial \hat{w}}{\partial \hat{x}} \right)^2 + \left(\frac{\partial \hat{w}}{\partial \hat{y}} \right)^2 \right) \right). \quad (2)$$

Since we assumed that $\delta \ll 1$ and the deformations are small, we neglect the δ^2 term on the right-hand side of eq. (2), and obtain an expression for the electrostatic force that depends only on the actual gap g . Thus, the validity of the analysis is limited to those variable gap capacitors whose actual gap is differentially uniform, that is, the two conductors are locally parallel to each other (see, *e.g.*, [4]).

We use the proximity force approximation (PFA) for the Casimir force f_c consistent with the assumptions made in the mechanical and the electrostatic models. In the PFA curved surfaces are viewed as a superimposition of infinitesimal parallel plates; see, *e.g.*, [18,19] and references therein. Gies and Klingmüller [19] have shown that for a sphere of radius R separated from a flat plate by a distance g , the PFA gives results within 1% accuracy for $g/R < 0.1$. By adopting the same nondimensionalization as before we have

$$f_c = -\frac{\hbar c \pi^2}{240 g_0^4 (1 + \hat{w})^4}, \quad (3)$$

where \hbar is Plank's constant and c the speed of light in the vacuum. Theoretical work has been devoted to estimating corrections to eq. (3) for geometries with known and fixed departures from the parallel configurations, see, *e.g.*, [18,19]. However, eq. (3) is consistent with the parallel-plate approximation for the electrostatic force, and the small deformations assumption in the mechanical model. As shown in [19], the PFA yields results within 0.1% error for the ratio $L/g \sim 10^2$.

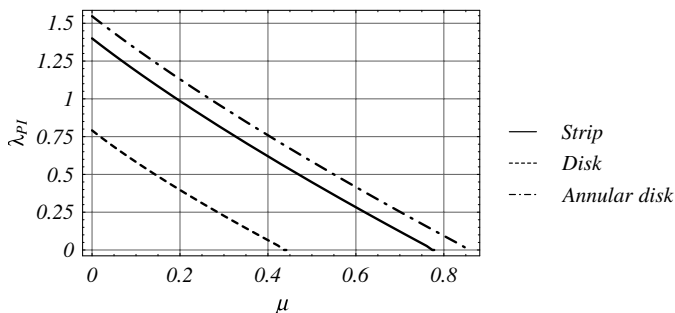
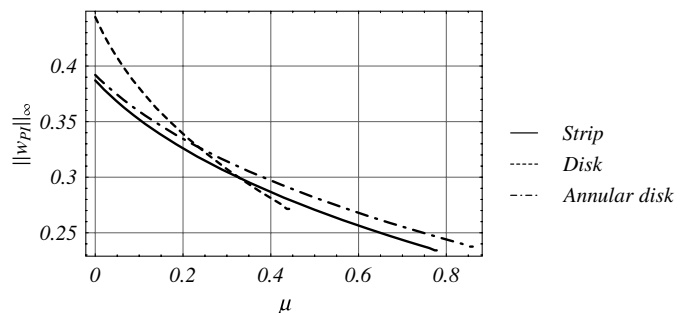
Under these assumptions, the equation in non-dimensional variables governing the deflection, w , of the device is

$$\Delta w(x, y) = \frac{\lambda}{(1 + w(x, y))^2} + \frac{\mu}{(1 + w(x, y))^4}, \quad (4)$$

where for convenience we have dropped the superimposed hat on w . The first and the second terms on the right-hand side of eq. (4) equal the Coulomb and the Casimir forces, respectively, and Δ is the Laplacian operator. Parameters λ and μ are defined by

$$\lambda = \frac{\epsilon_0 V^2 L^2}{2\sigma_0 h g_0^3}, \quad \mu = \frac{\hbar c L^2 \pi^2}{240 \sigma_0 h g_0^5}, \quad (5)$$

where σ_0 is the tension in the membrane. Note that the Coulomb force is proportional to V^2 but the Casimir force does not depend on V . As the voltage V increases, the parameter λ increases while μ stays constant. Both λ and μ depend upon the device dimensions through L^2/h . Whereas λ is inversely proportional to g_0^3 , μ is inversely


 Fig. 2: Pull-in parameter λ_{PI} vs. the Casimir force parameter μ .

 Fig. 3: Pull-in parameter $\|w_{\text{PI}}\|_{\infty}$ vs. the Casimir force parameter μ .

proportional to g_0^5 . Scaling down the device dimensions (h , g_0 , and L) by a factor F

$$h \rightarrow h/F, \quad g_0 \rightarrow g_0/F, \quad L \rightarrow L/F \quad (6)$$

increases λ by a factor of F^2 and μ by a factor of F^4 , that is

$$\lambda \rightarrow F^2 \lambda, \quad \mu \rightarrow F^4 \mu. \quad (7)$$

Thus, for $F > 1$, μ increases much faster than λ with a decrease in the device dimensions.

Effect of the scale on pull-in parameters. – We consider three sample geometries: a rectangular strip, a circular disk and an annular disk. The rectangular strip has length L and width $L/8$. The smaller edges are clamped and the other two are left free. The circular disk has radius L and is clamped along its periphery. The annular circular disk has outer radius L and inner radius $L/10$. It is clamped on both the inner and the outer perimeters.

We solve the nonlinear partial differential eq. (4) using the Meshless Local Petrov Galerkin method (MLPG) [20] in conjunction with the pseudoarclength continuation algorithm [21]. The MLPG method provides smooth and accurate solutions. The pseudoarclength method is suitable for analyzing multi-valued load-displacement diagrams and symmetry breaking.

The problem when solved for $\lambda = 0$ gives the critical value, μ_{cr} , of the Casimir force parameter. When $\mu = \mu_{\text{cr}}$ the system collapses spontaneously with zero applied voltage. The effect of the scale on pull-in parameters λ_{PI} and $\|w_{\text{PI}}\|_{\infty}$ is investigated by solving eq. (4) with variable λ for different values of μ in the range $[0, \mu_{\text{cr}}]$. The pull-in instability ($\lambda_{\text{PI}}, \|w_{\text{PI}}\|_{\infty}$) occurs when the curve $\|w\|_{\infty}(\lambda, \mu)$ becomes multi-valued.

In fig. 2 we report the pull-in parameter λ_{PI} versus μ for the three geometries. As μ increases the pull-in parameter λ_{PI} decreases monotonically from its maximum value $\lambda_{\text{PI}}^{\text{max}}$ corresponding to $\mu = 0$ to its minimum value 0 for $\mu = \mu_{\text{cr}}$. $\mu = \mu_{\text{cr}}$ represents intersection of the curves with the horizontal axis. The curves may be reasonably approximated by straight lines. Using this approximation, the knowledge of the pull-in parameter $\lambda_{\text{PI}}^{\text{max}}$ and of the critical Casimir parameter μ_{cr} are sufficient to completely

Table I: Characteristic parameters describing the influence of the Casimir force on pull-in instability.

Geometry	$\lambda_{\text{PI}}^{\text{max}}$	$\ w_{\text{PI}}\ _{\infty}^{\text{max}}$	μ_{cr}	$\ w_{\text{PI}}\ _{\infty}^{\text{min}}$
Strip	1.40	0.387	0.778	0.234
Disk	0.791	0.444	0.442	0.271
Annular disk	1.55	0.392	0.860	0.238

characterize the Casimir effect on the pull-in parameter λ_{PI} . The slopes of the three fitting straight lines are strikingly similar and approximately equal -1.8 .

In fig. 3 we show the nondimensional pull-in maximum displacement versus μ . We notice that as μ increases, the nondimensional maximum displacement decreases from its maximum value $\|w_{\text{PI}}\|_{\infty}^{\text{max}}$ for $\mu = 0$. This means that reduced deflection ranges are allowable for small devices. The minimum pull-in displacement $\|w_{\text{PI}}\|_{\infty}^{\text{min}}$ is attained when $\mu = \mu_{\text{cr}}$ and refers to the spontaneous collapse of the system without applied voltage.

Numerical values of $\lambda_{\text{PI}}^{\text{max}}$, $\|w_{\text{PI}}\|_{\infty}^{\text{max}}$, μ_{cr} , and $\|w_{\text{PI}}\|_{\infty}^{\text{min}}$ are summarized in table I. These reveal that the disk experiences the largest nondimensional pull-in maximum displacement and the maximum pull-in voltage is for the annular disk.

Analysis through a lumped model. – A qualitative analysis of the device may be conducted by using a simple lumped model proposed in [6]. The device is modeled as a parallel plate capacitor, where both plates are rigid. The upper plate is suspended by a linear spring, and the bottom plate is held fixed. \bar{w} is the displacement of the upper conductor, and it represents the maximum value of the displacement w of the distributed system. The reduced order model is

$$-\kappa \bar{w} = \frac{\lambda}{(1 + \bar{w})^2} + \frac{\mu}{(1 + \bar{w})^4}, \quad (8)$$

where κ is the nondimensional spring stiffness. The constant κ may be computed by solving a sample static problem on the distributed system without the Coulomb and the Casimir forces. Typically a uniformly distributed load on the movable conductor is considered, see,

Table II: Characteristic parameters describing the influence of the Casimir force parameter on the pull-in instability as predicted by the lumped model.

Geometry	Lumped model			% deviations	
	κ	$\lambda_{\text{PI}}^{\text{max}}$	μ_{cr}	$\lambda_{\text{PI}}^{\text{max}}$	μ_{cr}
Strip	8.00	1.18	0.655	15.7	15.8
Disk	4.00	0.593	0.328	25.0	25.7
Annular disk	8.80	1.30	0.721	16.1	16.1

e.g., [14,22]. In this case, the stiffness κ is equal to $1/\|w^*\|_{\infty}$, where w^* is the solution of

$$\Delta w^*(x, y) = 1 \quad (9)$$

with the proper boundary conditions. Values of κ for the strip, the disk and the annular disk are given in table II.

The pull-in instability is determined by imposing the force equilibrium (8) along with a subsidiary condition expressing that the restoring force is no longer capable of balancing the nonlinear attractive forces. This implies that the gap between the two plates changes without increasing the applied voltage. Mathematically this condition means that the derivative of both sides of eq. (8) with respect to \bar{w} are equal

$$\kappa = \frac{2\lambda}{(1+\bar{w})^3} + \frac{4\mu}{(1+\bar{w})^5}. \quad (10)$$

The solution of eqs. (8) and (10) can be written as

$$\frac{\lambda_{\text{PI}}}{\kappa} = \Lambda\left(\frac{\mu}{\kappa}\right), \quad \bar{w}_{\text{PI}} = -W\left(\frac{\mu}{\kappa}\right), \quad (11)$$

where Λ and W are nonlinear functions independent of κ . Figure 4 shows functions Λ and W for μ/κ in the range $[0, 256/3125]$. We note that $\Lambda(0) = 4/27$ and $\Lambda(256/3125) = 0$. For the three geometrical shapes considered here, the function Λ can be reasonably approximated by the straight line

$$\Lambda\left(\frac{\mu}{\kappa}\right) \simeq -1.8\frac{\mu}{\kappa} + 0.15. \quad (12)$$

The function W is monotonically decreasing. At $\mu = 0$, W equals $1/3$, while at $256/3125$ it equals $1/5$.

Pull-in displacements predicted by the distributed model significantly differ from those of the lumped model. In fact, the maximum pull-in deflection depends on the system geometry and boundary conditions, which are represented approximately in eq. (11) through κ . The deflection travel range $[1/3, 1/5]$ predicted by the lumped model is generally inaccurate.

Even if the influence of the Casimir parameter μ on the pull-in nondimensional voltage λ_{PI} is qualitatively described by the lumped model, predictions from it are

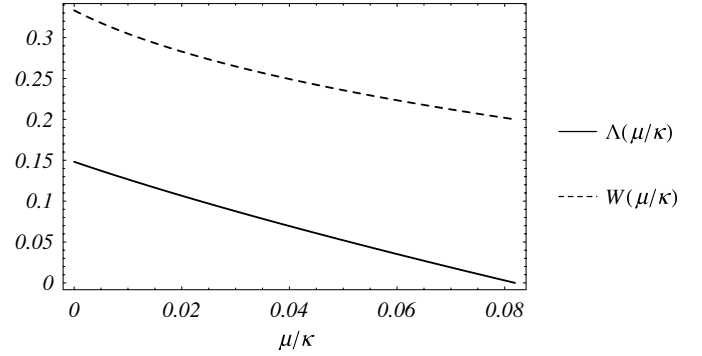


Fig. 4: Plots of functions Λ and W .

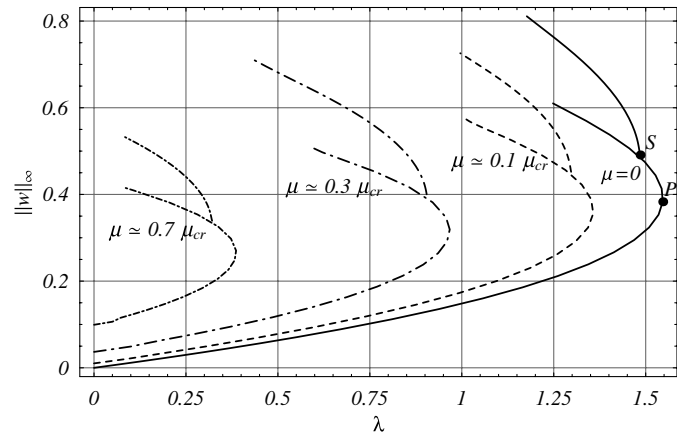


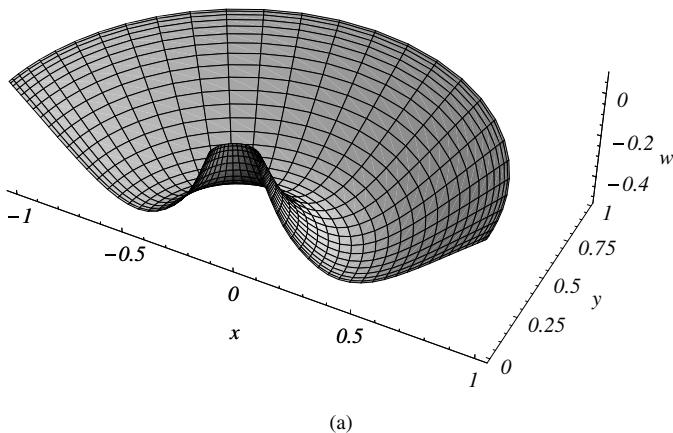
Fig. 5: Bifurcation diagrams of the annular membrane, for four different values of μ .

not accurate, as shown by comparison between results in table II with those in table I. For each geometry, the percentage deviations in $\lambda_{\text{PI}}^{\text{max}}$ and μ_{cr} computed from the distributed and the lumped models are the same. Thus the lumped model can be used to compare several preliminary (or prototype) designs of MEMS and the final few analyzed by the high-fidelity distributed models.

Effect of the scale on symmetry breaking. – We analyzed the post-instability behavior of the annular ring under effects of the Coulomb and the Casimir forces by solving the nonlinear eq. (4) for different values of μ in the range $[0, \mu_{\text{cr}}]$. We numerically studied one-half of the annular membrane, and imposed symmetry conditions on sides contiguous to the removed domain.

In fig. 5 we show the maximum deflection $\|w\|_{\infty}$ versus the voltage parameter λ for four different values of μ . For each value of μ the maximum deflection of the MEMS increases with an increase in λ and hence an increase in the applied voltage up to pull-in indicated by point P in fig. 5. This branch of the curve prior to the fold at P corresponds to stable equilibrium states, while the upper branch to unstable equilibrium states. At point S in fig. 5, besides the symmetric deformed configuration, asymmetric

$$\lambda = 0.0860, \mu = 0.618, \|w\|_\infty = 0.415$$



$$\lambda = 0.0842, \mu = 0.618, \|w\|_\infty = 0.532$$

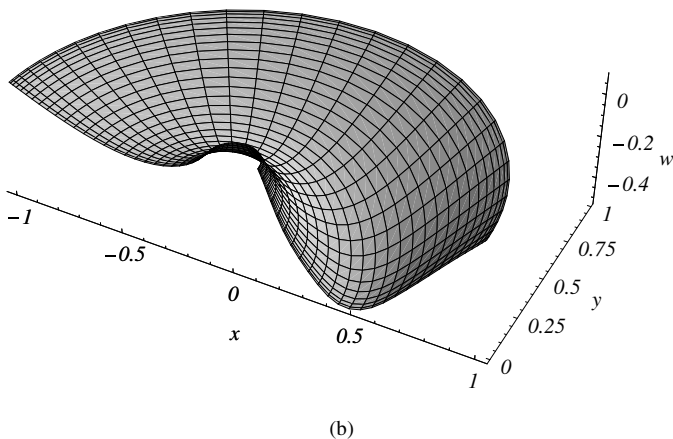


Fig. 6: Deformed shapes of the annular disk for $\mu \simeq 0.7\mu_{\text{cr}}$: (a) symmetric deformation; (b) asymmetric deformation.

deformed configuration corresponding to a point on the upper curve originating from S is also possible. For $\mu = 0.618$, those two configurations are reported in fig. 6 for two sets of values of λ and $\|w\|_\infty$. By considering one-half of the annular disk, we may have missed other non-axially symmetric deformation modes (see [23]).

If a micromembrane is pushed by forces other than the Coulomb force into a configuration corresponding to a point on the upper branch of the curves in fig. 5, eq. (4) and the prescribed boundary conditions are satisfied. The MEMS can theoretically stay in the unstable equilibrium configuration indefinitely if the external force is removed, the system is not perturbed, and the appropriate voltage is applied; see, *e.g.*, [11].

As the Casimir parameter μ varies, the bifurcation point $S(\lambda_{\text{SB}}, \|w_{\text{SB}}\|_\infty)$ moves, as listed in table III. Here λ_{SB} and w_{SB} equal, respectively, values of λ and w corresponding to the points where both symmetric and

Table III: Characteristic parameters describing symmetry breaking of the annular disk after pull-in instability.

μ/μ_{cr}	$\lambda_{\text{SB}}/\lambda_{\text{PI}}$	$\ w_{\text{SB}}\ _\infty/\ w_{\text{PI}}\ _\infty - 1$
0	0.960	0.282
0.101	0.956	0.270
0.332	0.935	0.254
0.718	0.831	0.255

asymmetric deformed configurations of the annular membrane are possible. As μ increases the ratio $\lambda_{\text{SB}}/\lambda_{\text{PI}}$ decreases, meaning that the difference in the nondimensional voltage corresponding to symmetry breaking and pull-in instability points increases. As μ increases the travel range of the device from the pull-in instability to the symmetry breaking point divided by the pull-in maximum deflection decreases eventually approaching a constant value.

An example. – Consider a circular membrane with parameters $L = 100 \mu\text{m}$, $g_0 = 1 \mu\text{m}$, $h = 0.1 \mu\text{m}$, $\sigma_0 = 10 \text{MPa}$. Substituting these values into eq. (5) gives $\mu = 8.17 \times 10^{-5}$ and the effect of the Casimir force is negligible, see fig. 4. Scaling down the device size by a factor $F = 10$, we have $\mu = 0.817$, which is larger than the critical Casimir parameter μ_{cr} in table I. This means that the miniaturized device spontaneously collapses under zero applied voltage. We note that the thickness of the scaled-down device equals 10 nm and we may be at the limit of applicability of the continuum theory. Also, van der Waals forces may play a role for the nano-scale device.

Detachment length. – The maximum length of the MEMS/NEMS that does not stick with the substrate without the application of a voltage is called the detachment length [14,24]. For a given initial gap g_0 the detachment length can be found by setting $\mu = \mu_{\text{cr}}$ in eq. (5). Using values of μ_{cr} listed in table I we get the maximum radius, L^{max} , of a circular MEMS that can be safely fabricated as $3.203 (\sigma_0 h g_0^5 / (\hbar c))^{1/2}$. For $h = 0.1 \mu\text{m}$, $g_0 = 1 \mu\text{m}$, $\sigma_0 = 10 \text{MPa}$, $L^{\text{max}} \simeq 7.2 \times 10^3 \mu\text{m}$. Conversely, for a given L , one can find the minimum initial gap, g_0^{min} , needed between the two parallel conductors for its safe fabrication to be $(\hbar c L^2 \pi^2 / (240 \sigma_0 h \mu_{\text{cr}}))^{1/5}$. With an increase in the initial tension σ_0 in the MEMS, L^{max} increases but g_0^{min} decreases. One can similarly find L^{max} and g_0^{min} for the annular disk and the rectangular strip.

Conclusions. – As the device size is reduced, the effect of the Casimir force becomes more important. In the miniaturization process there is a minimum size for the device below which the system spontaneously collapses with zero applied voltage.

A lumped model is capable of capturing the qualitative relationship between the pull-in voltage and the device size. We have given the simple closed form relation (12) that is suitable for a preliminary design of MEMS. The

accurate description of the relationship between the device travel range and the device scale, and the symmetry breaking in an annular disk after the pull-in instability necessitate the use of distributed models.

REFERENCES

- [1] NGUYEN C. T. C., KATEHI L. P. B. and REBEIZ G. M., *Proc. IEEE*, **86** (1998) 1756.
- [2] TILMANS H. A. and LEGTENBERG R., *Sensor. Actuator. A*, **45** (1994) 67.
- [3] HUNG E. S. and SENTURIA S. D., *J. Microelectromechanical Syst.*, **8** (1999) 497.
- [4] PELESKO J. A. and BERNSTEIN D. H., *Modeling MEMS and NEMS* (Chapman & Hall) 2002.
- [5] TAYLOR G. I., *Proc. Roy. Soc. A*, **306** (1968) 423.
- [6] NATHANSON H. C., NEWELL W. E., WICKSTROM R. A. and DAVIS J. R., *IEEE Trans. Electron Devices*, **306** (1968) 423.
- [7] LAMOREAUX S. K., *Rep. Progr. Phys.*, **68** (2005) 201.
- [8] BORDAG M., MOHIDEEN U. and MOSTEPANENKO V. M., *Phys. Rep.*, **353** (2001) 1.
- [9] LIFSHITZ E. M., *Sov. Phys. JETP*, **2** (1956) 73.
- [10] ZHAO Y.-P., WANG L. S. and YU T. X., *J. Adhesion Sci. Technol.*, **17** (2003) 519.
- [11] SERRY F. M., WALLISER D. and MACLAY G. J., *J. Appl. Phys.*, **84** (1998) 2501.
- [12] DING J.-N., WEN S.-Z. and MENG Y.-G., *J. Micromechanic. Microengineer.*, **72** (2001) 115426.
- [13] BÁRCENAS J., REYES L. and ESQUIVEL-SIRVENT R., *Appl. Phys. Lett.*, **87** (2005) 263106.
- [14] LIN W.-H. and ZHAO Y.-P., *Microsyst. Technol.*, **11** (2005) 80.
- [15] PALASANTZAS G. and DE HOSSON J. TH. M., *Phys. Rev. B*, **11** (2005) 202.
- [16] BAZERRA V. B., KLIMCHITSKAYA G. L. and MOSTEPANENKO V. M., *Phys. Rev. A*, **60** (2000) 014102.
- [17] KLIMCHITSKAYA G. L., ANUSHREE ROY, MOHIDEEN U. and MOSTEPANENKO V. M., *Phys. Rev. A*, **60** (1999) 3487.
- [18] BORDAG M., *Phys. Rev. D*, **73** (2006) 125018.
- [19] GIES H. and KLINGMÜLLER K., *Phys. Rev. Lett.*, **96** (2006) 220401.
- [20] ATLURI S. N. and SHEN S., *Comput. Model. Eng. Sci.*, **3** (2002) 11.
- [21] DOEDEL E., KELLER H. B. and KERNEVEZ J. P., *Int. J. Bifurcation Chaos*, **1** (1991) 493.
- [22] PAMIDIGHANTAM S., PUERS R., BAERT K. and TILMANS H. A. C., *J. Micromechanic. Microengineer.*, **12** (2002) 458.
- [23] PELESKO J. A., BERNSTEIN D. H. and MCCUAN J., *Proc. Model. Simul. Microsystems*, (2003) 304.
- [24] LIN W.-H. and ZHAO Y.-P., *Chin. Phys. Lett.*, **20** (2003) 2070.